6426 *Chem. Mater.* **2010,** *22,* 6426–6432
DOI:10.1021/cm102589x

CHEMISTRY OF MATERIALS
Article

Lithium Coordination Sites in Li_xTiO_2(B): A Structural and Computational Study

A. Robert Armstrong,[†] Corinne Arrouvel,[‡,§] Valentina Gentili,[†] Stephen C. Parker,[‡] M. Saiful Islam,[‡] and Peter G. Bruce*,[†]

[†]*EaStCHEM, School of Chemistry, University of St Andrews, St. Andrews, Fife, KY16 9ST, U.K.,* [‡]*Department of Chemistry, University of Bath, Bath, BA2 7AY, U.K., and* [§]*Universidade Federal de Sergipe, Departamento de Física, São Cristóvão, SE 49.100-000 Brazil*

Received September 9, 2010. Revised Manuscript Received November 2, 2010

A combination of powder neutron diffraction and computational methods, based on density functional theory (DFT), have been applied to study the evolution of structure with Li content for Li_xTiO_2(B) in bulk and nanowire form. Li_xTiO_2(B) is a promising anode material for rechargeable lithium batteries. Three structures were identified, $Li_{0.25}TiO_2$(B), $Li_{0.5}TiO_2$(B), and Li_xTiO_2(B), where x corresponds to the maximum Li content, 0.8 (bulk) and 0.9 (nanowires). Together the techniques demonstrate that at low lithium concentration (up to 0.25) the square planar lithium site at the center of the b axis channel (C site) is preferentially occupied. At higher concentration, ($Li_{0.5}TiO_2$(B)) the C site becomes unfavorable and the 5-coordinate A1 site is occupied, whereas at the highest Li content, both A1 and a further 5-coordinate site, A2, are occupied equally.

Introduction

Interest in rechargeable lithium batteries has reached new heights, in part, because of the demands of the automotive sector as it moves toward hybrid electric or pure electric vehicles.[1−3] New rechargeable lithium batteries containing new electrode materials are required. Graphite has been the dominant anode for rechargeable lithium batteries since their introduction in 1990.[4] However for large, high-power batteries, replacement of graphite by a titanate anode is receiving much attention.[5] The lithium intercalation potential of graphite is close to that of lithium plating leading to limited inherent overcharge protection .[6,7] In addition, the solid electrolyte interface (SEI) layer formed on graphite decomposes at ∼100 °C leading to safety problems on cell overheating. The higher voltage of the titanates (∼1.6 V vs Li) endows them with greater overcharge protection than graphite (avoiding Li plating). Also the material can be made in nanostructured form with a minimal SEI layer, thus permitting access to fast charge/discharge rates (high power). The higher anode voltage compromises the cell voltage and hence energy storage, although this can be offset by using higher voltage cathodes, for example, $LiNi_{0.5}Mn_{1.5}O_4$.[8]

The spinel, $Li_4Ti_5O_{12}$, has received most attention but can only store ∼175 mAh g^{-1}, approximately half the capacity of graphite but higher capacities are possible for nanomaterials.[9] TiO_2(B) as a bulk material can store 240 mAh g^{-1}; in nanowire form, this increases to 305 mAh g^{-1}, and for nanotubes, the capacity increases further to 330 mAh g^{-1} (corresponding to the composition $Li_{0.98}TiO_2$).[10] The only other polymorph that intercalates Li in the bulk is anatase (150 mAh g^{-1}), although all can do so in nanostructured form, even rutile.[11] As a result, TiO_2(B) is an attractive intercalation host for Li and hence as an anode for rechargeable lithium batteries. It is important to note that the density of the titanates is

*To whom correspondence should be addressed. E-mail: pgb1@st-and.ac.uk.

(1) Tarascon, J.-M.; Armand, M. *Nature* **2001**, *414*, 359.
(2) Whittingham, M. S. *Chem. Rev.* **2004**, *104*, 4271.
(3) Armand, M.; Tarascon, J.-M. *Nature* **2008**, *451*, 652.
(4) Nagaura, T.; Tozawa, K. *Prog. Batteries Sol. Cells* **1990**, *9*, 209.
(5) (a) Ferg, E.; Gummow, R. J.; De Kock, A.; Thackeray, M. M. *J. Electrochem. Soc.* **1994**, *141*, L147. (b) Ohzuku, T.; Ueda, A.; Yamamoto, N. *J. Electrochem. Soc.* **1995**, *142*, 1431. (c) Zaghib, K.; Simoneau, M.; Armand, M.; Gauthier, M. *J. Power Sources* **1999**, *81*, 300. (d) Nakahara, K.; Nakajima, R.; Matsushima, T.; Majima, H. *J. Power Sources* **2003**, *117*, 131. (e) Kavan, L.; Prochazka, J.; Spitler, T. M.; Kalbac, M.; Zukalova, M.; Drezen, T.; Grätzel, M. *J. Electrochem. Soc.* **2003**, *150*, A1000. (f) Reale, P.; Panero, S.; Scrosati, B.; Garche, J.; Wohlfahrt-Mehrens, M.; Wachtler, M. *J. Electrochem. Soc.* **2004**, *151*, A2138.
(6) Bruce, P. G. *Chem. Commun.* **1997**, 1817.
(7) Whittingham, M. S. *MRS Bull.* **2008**, *33*, 411.
(8) (a) Ariyoshi, K.; Yamamoto, S.; Ohzuku, T. *J. Power Sources* **2003**, *119*, 959. (b) Reale, P.; Panero, S.; Scrosati, B. *J. Electrochem. Soc.* **2005**, *152*, A1949.
(9) Borghols, W. J. H.; Wagemaker, M.; Lafont, U.; Kelder, E. M.; Mulder, F. M. *J. Am. Chem. Soc.* **2009**, *131*, 17786.
(10) (a) Armstrong, A. R.; Armstrong, G.; Canales, J.; Bruce, P. G. *Angew. Chem., Int. Ed.* **2004**, *43*, 2286. (b) Armstrong, A. R.; Armstrong, G.; Canales, J.; García, R.; Bruce, P. G. *Adv. Mater.* **2005**, *17*, 862. (c) Armstrong, G.; Armstrong, A. R.; Canales, J.; Bruce, P. G. *Electrochem. Solid-State Lett.* **2006**, *9*, A139. (d) Zukalová, M.; Kalbác, M.; Kavan, L.; Exnar, I.; Graetzel, M. *Chem. Mater.* **2005**, *17*, 1248.
(11) (a) Sudant, G.; Baudrin, E.; Larcher, D.; Tarascon, J.-M. *J. Mater. Chem.* **2005**, *15*, 1263. (b) Baudrin, E.; Cassaignon, S.; Koesch, M.; Jolivet, J. -P.; Dupont, L.; Tarascon, J.-M. *Electrochem. Commun.* **2007**, *9*, 337. (c) Wagemaker, M.; Borghols, W. J. H.; Mulder, F. M. *J. Am. Chem. Soc.* **2007**, *127*, 4323. (d) Reddy, M. A.; Kishore, M. S.; Pralong, V.; Varadaraju, U. V.; Raveau, B. *Electrochem. Solid-State Lett.* **2007**, *10*, A29. (e) Borghols, W. J. H.; Wagemaker, M.; Lafont, U.; Kelder, E. M.; Mulder, F. M. *Chem. Mater.* **2008**, *20*, 2949. (f) Hu, Y.-S.; Kienle, L.; Guo, Y.-G.; Maier, J. *Adv. Mater.* **2006**, *18*, 1421.

 Published on Web 11/17/2010

approximately twice that of graphite, thus doubling the energy density for the same specific energy.

Given the potential significance of TiO_2(B) it is important to establish how the structure changes on Li intercalation, especially the occupancy of Li sites over a range of Li concentrations. However, such structural details have not been fully characterized. In this work a combination of powder neutron diffraction and computational (DFT) studies have been employed to elucidate the structural changes in bulk and nanowire Li_xTiO_2(B) as a function of Li content. The thin walls of the TiO_2(B) nanotubes (2.5 nm), give rise to severe broadening of their powder diffraction patterns negating structure elucidation using established diffraction methods. However, their structure has been investigated using the Debye Method, which permits analysis of the powder diffraction pattern without recourse to translational symmetry. The structure is a distorted form of the bulk TiO_2(B) crystal structure.[12]

Experimental Section

Bulk TiO_2(B) was prepared via the layered precursor $K_2Ti_4O_9$. Stoichiometric amounts of K_2CO_3 (Fisher, 99%) and TiO_2 (anatase, Aldrich 99.8%) were ground using an agate mortar and pestle and calcined in air at 800 °C for 15 h. The product was reground and calcined for a second time under the same conditions to produce single phase $K_2Ti_4O_9$. Proton exchange to form isostructural $H_2Ti_4O_9$ was achieved by stirring at room temperature for 72 h in 3 M hydrochloric acid. The product was filtered, washed with distilled water and dried at 80 °C overnight. To form TiO_2(B) the resulting powder was annealed in air at 500 °C for 4 h.

Titanate nanowires were synthesized following our previously reported procedure.[10a] Anatase was added to a 15 M aqueous solution of NaOH. After the mixture was stirred for 1 h, the resulting suspension was transferred to a Teflon-lined autoclave and heated to 170 °C for 72 h. The product was acid-washed, which involved stirring the sample in 0.05 M HCl solution for 2 h. The material was then filtered, washed with distilled water, and dried at 80 °C for 15 h. TiO_2(B) nanowires were prepared by heating the acid-washed titanate nanowires at 400 °C for 4 h in air.

Lithiated samples for neutron diffraction were prepared both chemically and electrochemically. Chemical lithiation was carried out in an argon-filled glovebox using a solution of *n*-butyllithium (Aldrich, 1.6 M) in hexanes. The samples were stirred overnight, using stoichiometric amounts of *n*-butyllithium for low lithium contents and a 2-fold excess for full lithiation. The products were then filtered, washed with dry hexane and dried under vacuum. For neutron diffraction the samples were loaded into cylindrical vanadium cans (again under Argon). To prepare the electrochemically lithiated materials composite electrodes were constructed by mixing the active material, carbon, and Kynar Flex 2801 (a copolymer-based on PVdF) in the weight ratios 75: 18: 7 and pressing into pellets. The electrodes were incorporated into an electrochemical cell with a lithium metal counter electrode and the electrolyte was a 1 *m* solution of $LiPF_6$ in ethylene carbonate/dimethyl carbonate (1:1) (Merck). Electrochemical measurements were carried out using a Biologic MacPile II. Cells were stopped at various points on the first discharge and dismantled in an argon-filled glovebox. The electrodes were washed in dimethyl carbonate and the Kynar was dissolved in THF. The samples were then dried and loaded into 2 mm quartz capillaries for neutron diffraction measurements.

Powder X-ray diffraction data were collected on a Stoe STADI/P diffractometer operating in transmission mode with Cu$K\alpha_1$ radiation (λ = 1.54056 Å). Time-of-flight powder neutron diffraction data on the lithiated materials were obtained on the GEM and Polaris diffractometers at ISIS at the Rutherford Appleton Laboratory. The structures were refined by the Rietveld method using the program TOPAS Academic.[13] Chemical analysis was carried out using ICP.

Total energy calculations were performed within the framework of density functional theory (DFT) implemented in the Vienna Ab initio Simulation Package (VASP).[14] Different functionals have been previously tested on TiO_2(B)[15] and the generalized gradient approximation (GGA) of Perdew and Wang (PW91) was employed here.[16] The eigenstates of the electron wave functions are expanded on a plane-wave basis set using pseudopotentials to describe the electron-ion interactions within the projector-augmented wave (PAW) approach.[17] For total energy calculations, we used a cutoff energy of 500 eV to ensure a good description of the system. The Brillouin zone was sampled according to the Monkhorst−Pack scheme,[18] using a *k*-point grid up to 4 × 8 × 6 for geometric optimization of the $Li_xTi_8O_{16}$ cell.

We recognize that some recent studies on Ti-based oxides have used the DFT+U approach[19−22] to treat Ti oxidation states, although there are also numerous recent studies on defects in TiO_2,[23] and on lithium insertion in transition metal materials,[24] that have employed DFT-GGA methodology without the on-site U parameter. In this study our central aim is to investigate the lithium insertion sites in TiO_2(B), which are highly dependent upon the structural properties (especially unit cell volume) of the host lattice. It is known that the present GGA method has a small systematic overestimation of cell volumes. The greater structural difference for GGA+U leads to an incorrect Li insertion site stability for low Li content in which the Li−O distances at the C site are much longer, making this site unfavorable, which disagrees with experimental neutron diffraction studies. As detailed below, the DFT calculations with pure GGA (PW91) also result in better agreement with experimental cell voltages. These results are significant since it is known that U is usually fitted to reproduce some experimental property, in effect adding a semi-empirical component to the computations, as discussed by Nolan et al.[22] In short, our calculations on TiO_2(B) based on GGA-PW91

(12) Andreev, Y. G.; Bruce, P. G. *J. Am. Chem. Soc.* **2008**, *130*, 9931.
(13) Coelho, A. A. *J. Appl. Crystallogr.* **2000**, *33*, 899.
(14) (a) Kresse, G.; Hafner, J. *Phys. Rev. B* **1994**, *49*, 14251. (b) Kresse, G.; Furthmüller, J. *Comput. Mater. Sci.* **1996**, *6*, 15. (c) Kresse, G.; Furthmüller, J. *Phys. Rev. B* **1996**, *54*, 11169.
(15) Arrouvel, C.; Parker, S. C.; Islam, M. S. *Chem. Mater.* **2009**, *21*, 4778.
(16) Perdew, J. P.; Wang, Y. *Phys. Rev. B* **1992**, *45*, 13244.
(17) Kresse, G.; Joubert, D. *Phys. Rev. B* **1999**, *59*, 1758.
(18) Monkhorst, H. J.; Pack, J. D. *Phys. Rev. B* **1976**, *13*, 5188.
(19) Anisimov, V. I.; Zaanen, J.; Andersen, O. K. *Phys. Rev. B* **1991**, *44*, 943.
(20) Dudarev, S. L.; Botton, G. A.; Savrasov, S. Y.; Humphreys, C. J.; Sutton, A. P. *Phys. Rev. B* **1998**, *57*, 1505.
(21) Morgan, B. J.; Watson, G. W. *Surf. Sci.* **2007**, *601*, 5034.
(22) Nolan, M.; Elliot, S. D.; Mulley, J. S.; Bennett, R. A.; Basham, M.; Mulheran, P. *Phys. Rev. B* **2008**, *77*, 235424.
(23) (a) Graciani, J.; Ortega, Y.; Sanz, J. F. *Chem. Mater.* **2009**, *21*, 1431. (b) Yang, K. S.; Dai, Y.; Huang, B. B.; Whangbo, M. H. *Chem. Mater.* **2008**, *20*, 6528.
(24) (a) Anicete-Santos, M.; Gracia, L.; Beltran, A.; Andres, J.; Varela, J. A.; Longo, E. *Phys. Rev. B* **2008**, *77*, 085112. (b) Kang, K.; Morgan, D.; Ceder, G. *Phys. Rev. B* **2009**, *79*, 014305.

show good agreement with experiment for the unit cell volume, the favorable Li insertion site and the cell voltages without the use of an on-site U parameter, and hence this is the approach that we employed in the present study.

We will report the lithium intercalation energies, which can be represented by the following equations:

$$TiO_2 + xLi \rightarrow Li_xTiO_2 \quad (1)$$

$$E_{int} = \frac{E(Li_xTiO_2) - xE(Li) - E(TiO_2)}{x}$$

where $E(Li_xTiO_2)$ and $E(TiO_2)$ are the total energies of the lithiated bulk and unlithiated bulk of TiO_2 respectively. The energy of lithium metal, $E(Li)$ was obtained by optimization of body-centered cubic ($Im\bar{3}m$) Li metal with $a_0 = 3.491$ Å,[25] using a k-point mesh of $(25 \times 25 \times 25)$.

Such DFT techniques have been applied successfully to studies of other TiO_2 polymorphs[21,26] and oxide materials for lithium batteries in general.[27] Hitherto, there have been a few theoretical studies on TiO_2(B),[28] and it has been suggested that the Li 5-fold coordination sites in $Li_{0.75}TiO_2$(B) are similar to the sites in $Li_2FeV_3O_8$.[29] Recently, we have employed DFT methods to investigate Li insertion sites and diffusion pathways in TiO_2-(B) for low Li content ($x < 0.125$).[15] Panduwinata and Gale have also probed these issues and calculated that lithium is bound most favorably at a position close to the titania octahedral layer.[28d] Vittadini et al[28e] have used periodic DFT methods to investigate the structures and energetics of low-index surfaces of TiO_2(B). The present study also extends our recent computational studies of lithium ion transport and surface structures of $LiFePO_4$ cathode materials.[30]

Results

Crystal Structures of As-Prepared Bulk TiO_2(B) and TiO_2(B) Nanowires. The crystal structure of TiO_2(B) is monoclinic (space group $C2/m$) and is composed of edge and corner-sharing TiO_6 octahedra (Figure 1). The structures of the as-synthesized materials were refined using the model of Feist and Davies.[31] Beginning with bulk TiO_2(B), a good fit to the data was obtained, which could be further improved by incorporating *hkl*-dependent line-broadening, consistent with the rod-like morphology, observed even for bulk TiO_2(B). Broadening was primarily

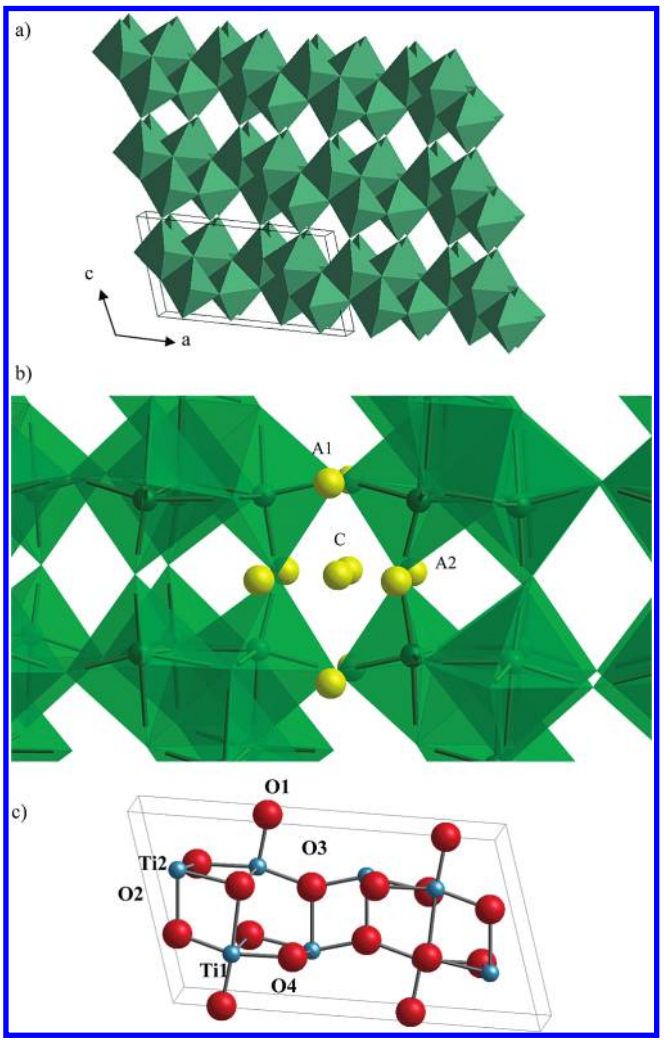

Figure 1. Bulk crystal structure of TiO_2(B) (a) TiO_6 octahedral units, (b) showing TiO_6 octahedra and lithium intercalation sites. (c) Ball and stick model showing atomic positions: oxygen atoms (red) and Ti atoms (blue).

associated with reflections perpendicular to the b direction in agreement with the alignment of the b axis of the unit cell along the length of the rod like morphology for bulk TiO_2(B). The coherence length in the radial direction is consistent with the diameter of the rods as determined by electron microscopy, ~100 nm. A profile fit to the data for bulk TiO_2(B) and the final refined parameters are given in Supporting Information (Figure S1a and table S1a).

In view of the significantly enhanced electrochemical properties observed for nanowires, we also examined the structure of this form of TiO_2(B). Again a good fit to the data was obtained, particularly with inclusion of *hkl*-dependent line-broadening in the model. In this case, the broadening was in the same direction as for the bulk but more severe, with a coherence length of 35 nm perpendicular to the $0k0$ unit cell direction in agreement with the diameter of ~30 nm for the wires, determined by TEM. The TEM data also confirmed that more than 95% of the material was composed of nanowires of similar diameter and with lengths up to 1 μm as shown in Figure 2. The profile fit and final refined parameters are shown in the Supporting Information (Figure S1b and Table S1b).

(25) Barrett, C. S. *J. Phys. Chem.* **1958**, *62*, 732.
(26) (a) Koudriachova, M. V.; Harrison, N. M.; de Leeuw, S. W. *Solid State Ionics* **2003**, *157*, 35. (b) Arrouvel, C.; Digne, M.; Breysse, M.; Toulhoat, H.; Raybaud, P. *J. Catal.* **2004**, *222*, 152.
(27) (a) Morgan, D.; Van der Ven, A.; Ceder, G. *Electrochem. Solid-State Lett.* **2004**, *7*, A30. (b) Zhou, F.; Cococcioni, M.; Marianetti, C. A.; Morgan, D.; Ceder, G. *Phys. Rev. B* **2004**, *70*, 235121. (c) Islam, M. S.; Davies, R. A.; Gale, J. D. *Chem. Mater.* **2003**, *15*, 4280.
(28) (a) Catlow, C. R. A.; Cormack, A. N.; Theobald, F. *Acta Crystallogr.* **1984**, *B40*, 195. (b) Swamy, V.; Gale, J. D.; Dubrovinsky, L. S. *J. Phys. Chem. Solids* **2001**, *62*, 887. (c) Nuspl, G.; Yoshizawa, K.; Yamabe, T. *J. Mater. Chem.* **1997**, *7*, 2529. (d) Panduwinata, D.; Gale, J. D. *J. Mater. Chem.* **2009**, *19*, 3931. (e) Vittadini, A.; Casarin, M.; Selloni, A. *J. Phys. Chem. C* **2009**, *113*, 18973.
(29) Tournoux, M.; Marchand, R.; Brohan, L. *Prog. Solid State Chem.* **1986**, *17*, 33.
(30) (a) Islam, M. S.; Driscoll, D. J.; Fisher, C. A. J. *Chem. Mater.* **2005**, *17*, 5085. (b) Fisher, C. A. J.; Islam, M. S. *J. Mater. Chem.* **2008**, *18*, 1209.
(31) Feist, T. P.; Davies, P. K. *J. Solid State Chem.* **1992**, *101*, 275.

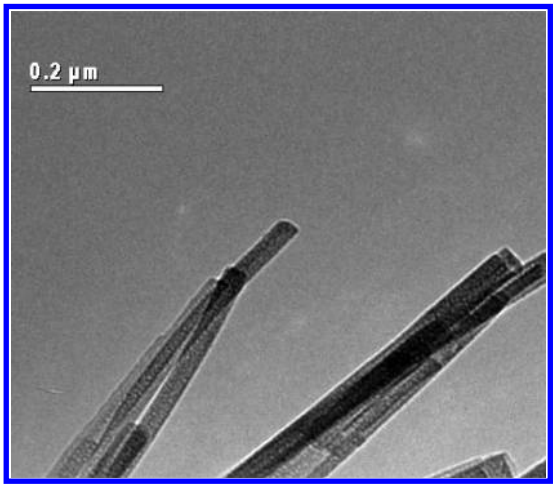

Figure 2. Low-resolution TEM image of the TiO_2(B) nanowires.

To probe the validity of our computational approach, structural optimizations of TiO_2(B) were performed based on the experimentally observed bulk crystal structure. The unit cell volume was fully relaxed, while maintaining the overall shape of the cell in which the a/b and c/b ratios were kept constant. The calculated and experimental structural parameters are listed in the Supporting Information and show good accord for the unit cell parameters and atom positions (Table S2).

Load Curves. The variations of voltage with Li content for bulk and nanowire TiO_2(B) are presented in Figure 3a. As expected the voltages for the two materials are similar. The curves are not smooth functions of Li content; instead a series of plateaus and sloping regions may be identified, the former corresponding to two-phase regions and the latter to solid solutions. The location of the plateaus are more clearly seen in the differential capacity plots in Figure 3b, where three peaks (corresponding to the three plateaus on the load curves) are evident. Although the plateau voltages are clearly identified in the differential capacity plots the composition ranges which the two-phase regions span are difficult to establish from the load curves. As a result it is difficult to identify the exact compositions of the single-phase, stoichiometric, end members for structure elucidation. The only exception was the highest Li content, where the load curves are clearly sloping and where we observe a single phase.

$Li_{0.25}TiO_2$(B). As noted previously, in evaluating the influence of insertion processes on the structural and transport properties of the TiO_2(B) host material, it is important to know the precise location of the lithium ions, which can be difficult to extract from X-ray diffraction experiments. Brohan and Marchand have described some possible intercalation sites in the TiO_2(B) structure, labeled C, A1, and A2 (shown in Figure 1).[32] The C site is at the center of the large channels along the b-axis, surrounded by a square-planar arrangement of oxygen atoms. The A1 site is 5-fold coordinated within the (001) plane and is also present in $Li_2FeV_3O_8$. The A2 site is also

(32) Brohan, L.; Marchand, R. *Solid State Ionics* **1983**, *9*−*10*, 419.

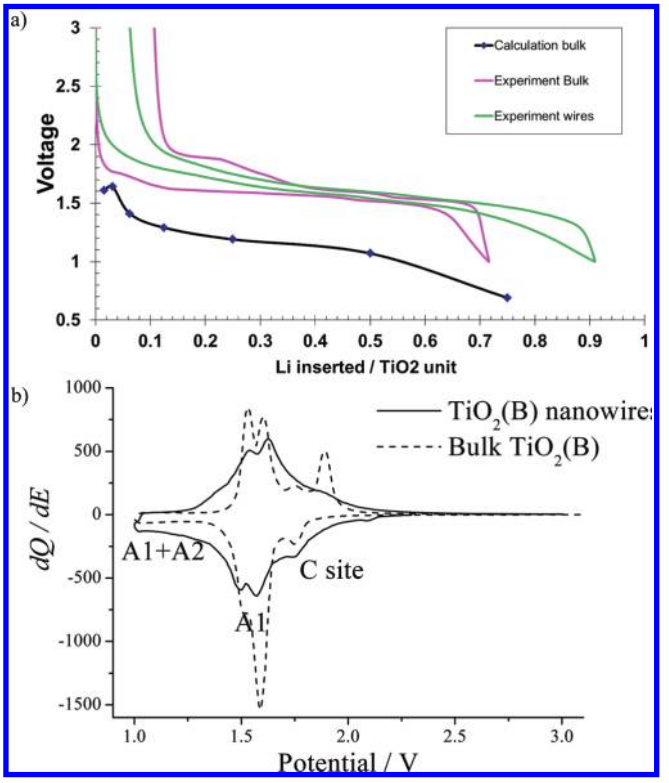

Figure 3. (a) Experimental and calculated variation of potential, vs Li/Li^+ (1 M) electrode, with Li content (charge passed) for bulk and nanowire TiO_2(B). (b) Incremental capacity plots for bulk TiO_2(B) and TiO_2(B) nanowires cycled at 10 mA g^{-1} between voltage limits of 1 and 3 V. The Li coordination sites associated with each potential are indicated.

a 5-fold site and lies between the oxygens (O_{br}) that bridge adjacent layers in the (001) plane.

A chemically lithiated sample of bulk Li_xTiO_2(B) with the composition $x = 0.15$ was examined using neutron diffraction. It was clear that the data could not be fitted satisfactorily to a single TiO_2(B)-based phase, rather, two such phases were necessary. These correspond to as-prepared TiO_2(B) and $Li_{0.25}TiO_2$(B). The presence of two phases at an average Li content of 0.15 is not in keeping with the load curves (Figure 3a), which instead suggest that this composition corresponds to the end of a single-phase region and the beginning of a plateau. Inhomogeneity is not unexpected in chemically prepared samples, especially at modest Li contents. The diffraction data are consistent with lithium intercalation into only a proportion of the material resulting in a mixture of unreacted TiO_2(B) and $Li_{0.25}TiO_2$(B). The Li coordination site of the latter was established by refinement and the Li^+ was found to occupy the channel site, C. In fact the position of Li in the C site is slightly off-center, displaced along the b-axis. This represents the limiting stoichiometry corresponding to full occupation of the C-site. A fit to the data is shown in Figure 4, and the final refined parameters for the $Li_{0.25}TiO_2$(B) end member are given in Table 1. Of interest is the anisotropic expansion that occurs on lithium insertion, with a showing significant increase, b a moderate increase, while c exhibits a slight contraction.

Considering the DFT calculations, the relative occupancies of the possible sites were examined by calculating

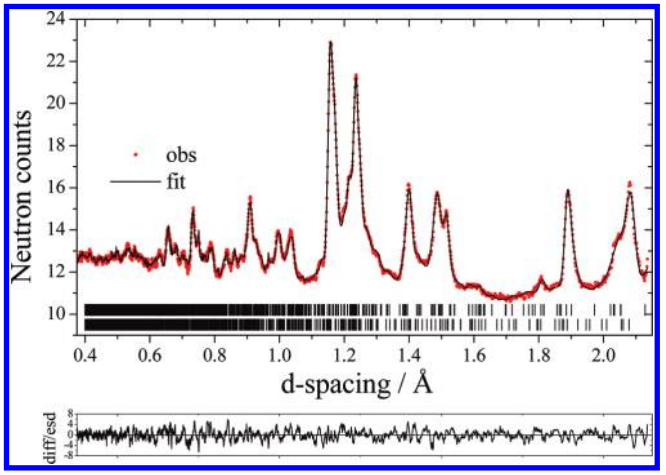

Figure 4. Refined powder neutron diffraction pattern for $Li_{0.15}TiO_2$(B) using a two phase model with *hkl* dependent line broadening. Dots represent observed data and solid line the calculated pattern. The lower line is the difference/esd. Upper tick marks represent allowed reflections for $Li_{0.25}TiO_2$(B), while lower tick marks are from TiO_2(B).

the energies for lithium interstitial ions at the various insertion sites (C, A1, and A2) within the TiO_2(B) structure. For these constant pressure calculations, the unit cell volume and atom positions of the host oxide were allowed to relax after lithium insertion. For compositions $x < 0.25$ and assuming a single-phase model, the relative energies suggest that the C site is most favorable for Li^+ insertion by more than 90 meV. The calculations also find that the Li position for the C site is slightly off-center by ca. 0.4 Å along the *b* axis, in good accord with the diffraction study.

$Li_{0.5}TiO_2$(B). A sample prepared chemically with $x = 0.4$ was examined in this composition window. Again the diffraction pattern best fitted two phases, a mixture of $Li_{0.25}TiO_2$(B) and $Li_{0.5}TiO_2$(B), in keeping with the load curves in Figure 3. As indicated above, insertion of lithium beyond $x = 0.25$ must necessarily result in occupancy of an additional coordination site. However, in practice what is observed is a complete depopulation of the C-site, with lithium exclusively occupying the 5-coordinate A1 site in $Li_{0.5}TiO_2$(B). A fit to the data is shown in Figure 5 with refined parameters in Table 2. Our calculations also indicate that for Li concentrations $x \geq 0.25$, the C site is no longer favorable. For $x = 0.5$, the relative energies for Li insertion at the A1 and A2 sites suggest that the A1 site is now the most favorable by over 110 meV. Indeed, all the configurations for $x > 0.25$ with any C-site occupancy are the least favorable.

By discharging a cell to 1.55 V, between the two reduction peaks in Figure 3b, corresponding to a composition close to $x = 0.5$, diffraction data were collected that are well described by single phase $Li_{0.5}TiO_2$(B), Supporting Information Figure S2. This corroborates the structure refined in the 2-phase region. The nanowire form of TiO_2(B) was also intercalated to $x = 0.4$ and found to behave in a similar manner, that is, the same two phases were present, $Li_{0.25}TiO_2$(B) and $Li_{0.5}TiO_2$(B), Supporting Information Figure S3 .

Li_xTiO_2(B), $0.5 < x < 1$. The maximum Li content that could be obtained, chemically or electrochemically,

Table 1. Refined Structural Parameters for Bulk $Li_{0.25}TiO_2$(B)[a]

atom	Wyckoff symbol	*x*/*a*	*y*/*b*	*z*/*c*	B_{iso}	occupancy
Ti1	*4i*	0.3057(15)	0.0	0.691(3)	0.32(6)	1
Ti2	*4i*	0.4139(18)	0.0	0.305(3)	0.32(6)	1
O1	*4i*	0.3393(12)	0.0	0.994(2)	0.46(3)	1
O2	*4i*	0.2317(12)	0.0	0.339(2)	0.46(3)	1
O3	*4i*	0.1227(11)	0.0	0.714(2)	0.46(3)	1
O4	*4i*	0.4266(9)	0.0	0.672(2)	0.46(3)	1
Li1	*4g*	0.0	0.33(2)	0	0.4	0.5

[a] Space group *C*2/*m*, $a = 12.884(5)$ Å, $b = 3.8019(8)$ Å, $c = 6.501(2)$ Å, $\beta = 108.72(4)^o$, vol = 301.6 Å^3, $R_e = 0.62\%$, $R_{wp} = 1.15\%$, $R_p = 0.93\%$ for 2-phase refinement of $Li_{0.15}TiO_2$(B).

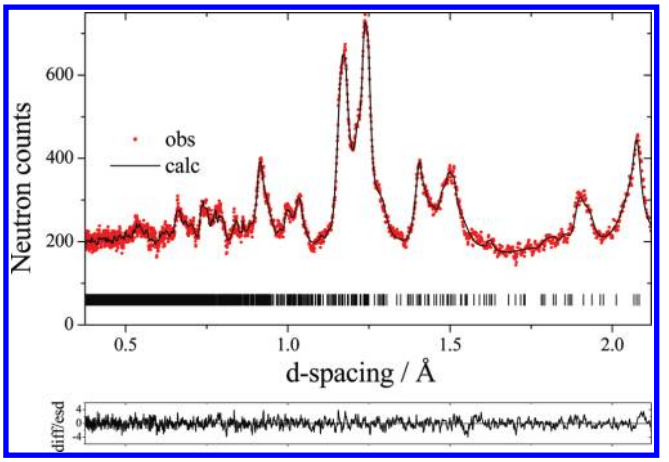

Figure 5. Refined powder neutron diffraction pattern for $Li_{0.4}TiO_2$(B). Dots represent observed data and solid line the calculated pattern. The lower line is the difference/esd. Tick marks represent allowed reflections for $Li_{0.5}TiO_2$(B).

Table 2. Refined Structural Parameters for Bulk $Li_{0.5}TiO_2$(B)[a]

atom	Wyckoff symbol	*x*/*a*	*y*/*b*	*z*/*c*	B_{iso}	occupancy
Ti1	*4i*	0.3128(16)	0.0	0.694(3)	0.1(1)	1
Ti2	*4i*	0.3991(17)	0.0	0.318(3)	0.1(1)	1
O1	*4i*	0.3508(14)	0.0	0.002(2)	0.41(5)	1
O2	*4i*	0.2325(12)	0.0	0.337(2)	0.41(5)	1
O3	*4i*	0.1270(11)	0.0	0.697(2)	0.41(5)	1
O4	*4i*	0.4507(14)	0.0	0.634(2)	0.41(5)	1
Li1	*4i*	0.928(3)	0.0	0.669(8)	0.4	1

[a] Space group *C*2/*m*, $a = 12.451(5)$ Å, $b = 3.8168(8)$ Å, $c = 6.456(3)$ Å, $\beta = 107.78(3)^o$, vol = 295.2 Å^3, $R_e = 3.61\%$, $R_{wp} = 5.48\%$, $R_p = 4.54\%$.

corresponded to the compositions, $Li_{0.8}TiO_2$(B) and $Li_{0.9}TiO_2$(B), for the bulk and nanowires, respectively. The diffraction patterns in both cases are well described by single phase models, Figures 6 and 7 and Tables 3 and 4, although a misfit in the former at around 1.5 Å *d*-spacing may stem from a small amount of lithiated anatase impurity. Insertion of lithium beyond $x = 0.5$ was found to result in occupation of a new coordination site, A2, also with 5-coordinate lithium. The A1 site, which was fully occupied in the $Li_{0.5}TiO_2$(B) material, is partially occupied in the Li-rich compositions along with partial occupancy of the A2 sites. The calculations also indicate that the most favorable insertion energies for $x > 0.5$ are for the A1 and A2 sites; the energy

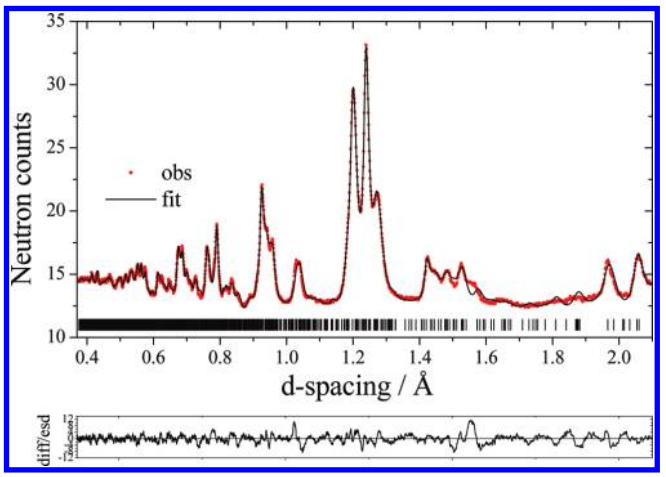

Figure 6. Refined powder neutron diffraction pattern for $Li_{0.8}TiO_2(B)$. Dots represent observed data and solid line the calculated pattern. The lower line is the difference/esd. Tick marks represent allowed reflections.

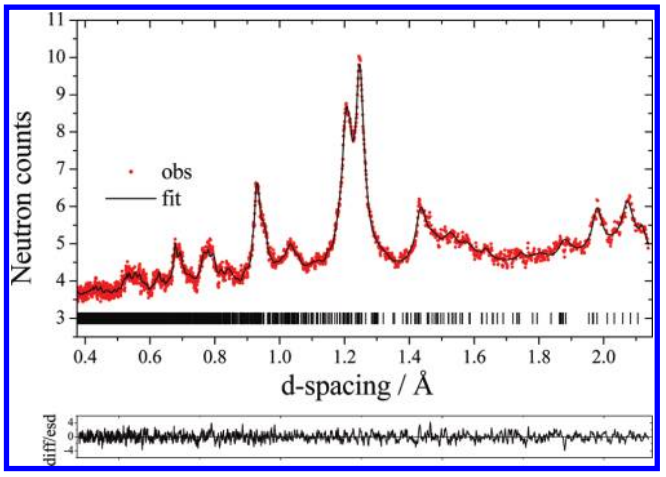

Figure 7. Refined powder neutron diffraction pattern for nanowire $Li_{0.9}TiO_2(B)$. Dots represent observed data and solid line the calculated pattern. The lower line is the difference/esd. Tick marks represent allowed reflections.

differences between these two sites of ~10 meV are less than kT and hence indicate that both A1 and A2 would be occupied as observed. It is interesting to note that the volume change for the nanowires is rather smaller than that observed in the bulk.

Voltages. The average experimental voltage for bulk or nanowire $TiO_2(B)$ is usually considered to be ~1.6 V vs Li^+ (with the voltage being measured at $x = 0.5$), Figure 3a.

Previous DFT studies of a wide variety of Li-intercalated transition metal compounds have indicated that the average cell voltage can be derived using these theoretical methods.[33,34] Here we wish to derive a reliable comparison of cell voltages as a function of lithium content in bulk $TiO_2(B)$. The total energies from a series of structural optimizations for a range of $Li_xTiO_2(B)$ compositions indicated in Figure 3a were used.

(33) Braithwaite, J. S.; Catlow, C. R. A.; Harding, J. H.; Gale, J. D. *Phys. Chem. Chem. Phys.* **2001**, *3*, 4052.
(34) Reed, J.; Ceder, G. *Electrochem. Solid-State Lett.* **2002**, *5*, A145.

Table 3. Refined Structural Parameters for Bulk $Li_{0.8}TiO_2(B)$[a]

atom	Wyckoff symbol	x/a	y/b	z/c	B_{iso}	occupancy
Ti1	*4i*	0.2996(11)	0.0	0.6906(15)	0.31(6)	1
Ti2	*4i*	0.4017(14)	0.0	0.3215(19)	0.31(6)	1
O1	*4i*	0.3418(7)	0.0	0.9983(15)	0.25(2)	1
O2	*4i*	0.2341(8)	0.0	0.3488(10)	0.25(2)	1
O3	*4i*	0.1272(6)	0.0	0.6774(11)	0.25(2)	1
O4	*4i*	0.4428(8)	0.0	0.6662(12)	0.25(2)	1
Li1	*4i*	0.935(2)	0.0	0.641(3)	0.4	0.75(5)
Li2	*4i*	0.185(2)	0.0	0.008(4)	0.4	0.85(5)

[a] Space group $C2/m$, $a = 12.7799(18)$ Å, $b = 3.9319(3)$ Å, $c = 6.5128(8)$ Å, $\beta = 108.89(2)^o$, vol = 309.6 Å^3, $R_e = 0.57\%$, $R_{wp} = 1.44\%$, $R_p = 1.07\%$.

Table 4. Refined Structural Parameters for Nanowire $Li_{0.9}TiO_2(B)$[a]

atom	Wyckoff symbol	x/a	y/b	z/c	B_{iso}	occupancy
Ti1	*4i*	0.295(2)	0.0	0.668(5)	0.6(2)	1
Ti2	*4i*	0.414(2)	0.0	0.317(4)	0.6(2)	1
O1	*4i*	0.3449(12)	0.0	0.993(3)	0.33(6)	1
O2	*4i*	0.2252(17)	0.0	0.346(3)	0.33(6)	1
O3	*4i*	0.1269(14)	0.0	0.685(2)	0.33(6)	1
O4	*4i*	0.4399(16)	0.0	0.649(3)	0.33(6)	1
Li1	*4i*	0.964(4)	0.0	0.661(9)	0.4	0.95(9)
Li2	*4i*	0.162(5)	0.0-	−0.007(11)	0.4	0.85(9)

[a] Space group $C2/m$, $a = 12.513(7)$ Å, $b = 3.9361(8)$ Å, $c = 6.493(2)$ Å, $\beta = 108.12(4)^o$, vol = 303.6 Å^3, $R_e = 2.29\%$, $R_{wp} = 2.76\%$, $R_p = 2.27\%$.

At each composition, we employed the structure with the favored Li site occupancies, discussed above. As with previous studies based on DFT-GGA, the quantitative discrepancy is consistent with the systematic underprediction of the cell potential in transition metal oxides.[33,34] In this case, the voltage range is about 0.69−1.61 V. The general shape, but not the absolute values, of the calculated voltage curve follows the experimental data. Thus the favored Li site occupancies from the calculations lead to a consistent trend in cell voltages as a function of Li content.

Conclusion

A combination of structural studies using powder neutron diffraction and computational studies based on DFT methods have aided our understanding of the lithium insertion sites in the $TiO_2(B)$ electrode material as a function of lithium content. The following main points emerge from our study.

(1) The most favorable lithium insertion site at low concentration ($x < 0.25$ for $Li_xTiO_2(B)$) is found in the [010] channel at the square planar site (termed the C-site) with a slightly off center position. At higher Li content, the C site becomes unfavorable. For $0.25 \le x \le 0.5$, the 5-coordinate A1 site is occupied, whereas at $x = 1$, both A1 and A2 sites are fully occupied.

(2) The volume and the shape of the unit cell vary with the Li concentration. There is an increase of the

cell volume with the Li content and an anisotropic variation of the cell parameters including a pronounced expansion along the *b* direction.

(3) The calculated variation of cell voltages, although not the absolute values, based on the favored Li site occupancies is consistent with the experimental profiles. For the incremental capacity plots, the potential regions can be associated with the Li^+ occupying the different coordination sites.

(4) TiO_2(B) bulk and nanowires are found to show similar behavior.

Acknowledgment. We would like to acknowledge the EPSRC for funding as a part of the Supergen Energy Storage Consortium (Grant EP/D031672/1). The computer facilities used are HECToR within the Materials Chemistry Consortium (Grant EP/F067496/1). C.A. acknowledges CNPq and FAPITEC for support.

Supporting Information Available: Tables showing refined structural parameters for as-prepared bulk TiO_2 and TiO_2 nanowires and calculated structural parameters of TiO_2 (B) bulk and figures showing powder neutron diffraction patterns. This material is available free of charge via the Internet at http://pubs.acs.org.